

Production and fate of the G ring arc particles due to Aegaeon (Saturn LIII)

Gustavo Madeira,[★] R. Sfair,[★] D. C. Mourão and S. M. Giuliatti Winter[★]

Univ. Estadual Paulista -UNESP, Grupo de Dinâmica Orbital e Planetologia, Guaratinguetá, CEP 12516-410, Brazil

Accepted 2018 January 8. Received 2018 January 5; in original form 2017 June 29

ABSTRACT

The G ring arc hosts the smallest satellite of Saturn, Aegaeon, observed with a set of images sent by Cassini spacecraft. Along with Aegaeon, the arc particles are trapped in a 7:6 corotation eccentric resonance with the satellite Mimas. Due to this resonance, both Aegaeon and the arc material are confined to within 60° of corotating longitudes. The arc particles are dust grains which can have their orbital motions severely disturbed by the solar radiation force. Our numerical simulations showed that Aegaeon is responsible for depleting the arc dust population by removing them through collisions. The solar radiation force hastens these collisions by removing most of the $10\ \mu\text{m}$ sized grains in less than 40 yr. Some debris released from Aegaeon's surface by meteoroid impacts can populate the arc. However, it would take 30 000 yr for Aegaeon to supply the observed amount of arc material, and so it is unlikely that Aegaeon alone is the source of dust in the arc.

Key words: planets and satellites: rings.

1 INTRODUCTION

Before the discovery of the small satellite Aegaeon, a bright arc close to the inner edge of Saturn's G ring was imaged by the cameras onboard the Cassini spacecraft. Located at about 167 500 km from Saturn's centre, this arc extends over $\sim 60^\circ$ in longitude and has a radial width of 250 km, while the rest of the G ring is 6000 km wide (Hedman et al. 2007). Cassini data showed that most of the arc is populated by micrometre-sized dust grains, although larger bodies (cm to metres in size) can also be present. Hedman et al. (2007) argued that a decrease in the flux of energetic electrons, observed by the Cassini instruments, could be caused by a population of cm-m sized bodies. They proposed that these large bodies could be the source of the arc and also the G ring.

The mean motion of the arc is close to the 7:6 corotation eccentric resonance (CER) with Mimas (Hedman et al. 2007). The resonant argument $\phi = 7\lambda_M - 6\lambda - \varpi_M$ is equal to 180° , where λ_M and λ are the mean longitudes of Mimas and the particle, respectively, and ϖ_M is the longitude of Mimas' pericentre. Hedman et al. (2007) numerically simulated a sample of particles initially located in this arc and verified that they stay confined for at least 80 yr.

Several Cassini images taken between 2007 and 2009 showed a small satellite, named Aegaeon, embedded in the G ring arc. With a diameter about 500 m, Aegaeon is trapped in the same 7:6 corotation eccentric resonance with Mimas with a libration amplitude of about 10° (Hedman et al. 2010).

In this work, we analyse the influence of Aegaeon on the small particles located in the G ring arc, after their possible ejection from the surface of Aegaeon, as well as their orbital evolution due to gravitational and dissipative forces. In Section 2, we analyse the orbital evolution of a set of micrometre-sized particles under the effects of the solar radiation force and the gravitational effects of the planet and the saturnian satellites, Mimas, Tethys, and Aegaeon. In Section 3, we analyse the time evolution of those dust particles ejected from the surface of the small satellite. Section 4 compares these estimates of dust lifetimes with the production rate due to impacts on to Aegaeon's surface in order to analyse the role of the satellite on the maintenance of the arc population. Our results are discussed in the last section.

2 ORBITAL EVOLUTION OF THE G RING ARC PARTICLES

First of all, we analyse the gravitational effects of Mimas on the particles located in the G ring arc. The dynamical system is formed by Saturn, including the gravitational coefficients J_2 , J_4 , and J_6 , and the satellites Mimas, Aegaeon, and Tethys. The numerical simulations were performed using the Mercury integrator package (Chambers 1999) with the Burlish Stör algorithm. We also used the algorithm described in Renner & Sicardy (2006) to convert the state vector into the geometric orbital elements that account for the orbital precession caused by the gravity coefficients of Saturn. Table 1 shows the initial osculating elements (2 454 700.5 JD), mass and density of the satellites, while Table 2 presents the parameters of Saturn: radius (in km), mass (in kg) (Thomas et al. 2013), J_2 , J_4 , and J_6 [consistent with Hedman et al. (2010)].

[★] E-mail: gtmadeira@gmail.com (GM); rsfair@gmail.com (RS); giuliattiwinter@gmail.com (SMGW)

Table 1. Mass (m), density (d) and osculating elements of the satellites (2 454 700.5 JD): a is the semimajor axis, e is the eccentricity, I is the inclination, and the angles ϖ , Ω , and λ are the argument of pericentre, longitude of node, and mean anomaly, respectively. These values were extract from JPL-Horizons System.

	Aegaeon	Mimas	Tethys
a ($\times 10^5$ km)	1.680 339 681 9	1.860 046 687 9	2.949 742 648 8
e ($\times 10^{-2}$)	0.312 128 572 7	1.724 521 920 9	0.082 811 658 1
I ($^\circ$)	0.001 476 108 7	1.568 757 162 0	1.091 516 297 3
ϖ ($^\circ$)	145.762 805 92	163.180 239 84	15.906 312 542
Ω ($^\circ$)	233.022 111 68	259.152 584 36	355.420 831 94
λ ($^\circ$)	5.359 424 904 5	197.732 789 53	4.522 131 857 0
m (kg)	5.997×10^{10}	3.754×10^{19}	61.760×10^{19}
d (g cm $^{-3}$)	0.500	1.152	0.956

Table 2. Physical parameters of Saturn.

Radius (km)	603 30
Mass ($\times 10^{26}$ kg)	5.686 837 654 95
J_2 ($\times 10^{-6}$)	16 290.543 820
J_4 ($\times 10^{-6}$)	−936.700 366
J_6 ($\times 10^{-6}$)	86.623 065

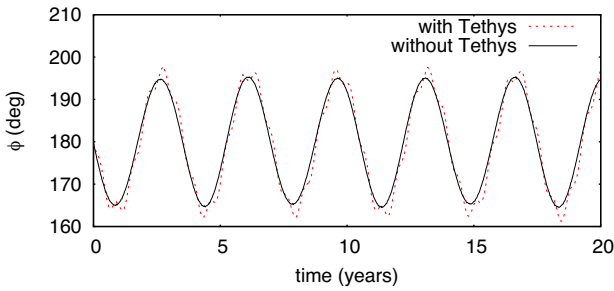


Figure 1. Resonant argument of Aegaeon as a function of time with (dashed line) and without the gravitational effects of Tethys. Tethys disturbs the resonant angle of Aegaeon.

The resonant argument of Aegaeon as a function of time is showed in Fig. 1. Gravitational effects of the satellite Tethys induce small variations in the resonant argument which can be seen in Fig. 1 (dashed line). Although these small variations did not alter the lifetime of the particles, the effects of Tethys were added to the system just for completeness.

A sample of 6000 test particles was randomly distributed, with uniform probability, in a resonant arc confined 60 km in radius and 60° azimuthally. The initial orbital elements, e , I , ω , and Ω , of the particles have the same values of the initial orbital elements of Aegaeon (Table 1). This sample of particles was used in all numerical simulations described in this section. When the distance between the particle and Aegaeon is less than the radius of the small satellite ($r = 240$ m, Hedman et al. 2010), a collision is detected.

Our numerical simulations for a time span of 500 yr showed that the particles, due to Mimas 7:6 CER, are azimuthally confined in the arc with an amplitude of 60° . Fig. 2 presents the geometric semimajor axis as a function of time of Aegaeon and eight arc particles. These particles are initially displaced by 5, 15, 25, and 35 km from the resonant semimajor axis (167 493.73 km). Although the particles displaced by 5–25 km from Aegaeon’s semimajor axis show some variation in the semimajor axis, they remain located in the arc region. The 7:6 CER with Mimas has a width of about 60 km

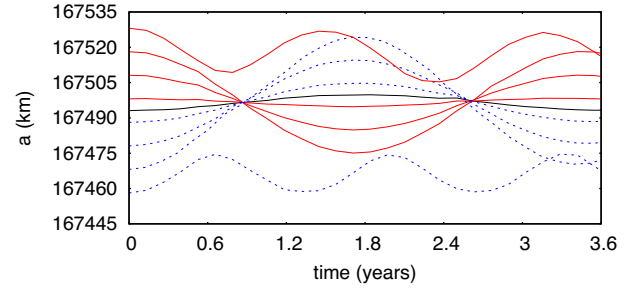


Figure 2. This figure shows the geometric semimajor axis (in km) as a function of time (in years) of Aegaeon and eight particles near the outer (full line) and inner (dashed line) edges of the arc.

(El Moutamid, Sicardy & Renner 2014), therefore those particles displaced by more than 30 km from the resonant semimajor axis are not azimuthally confined.

Besides the gravitational effects of Mimas on the arc particles, the small satellite Aegaeon also causes small variations in their orbital elements. Variations in the geometric eccentricity and inclination of the particles are of order 10^{-6} , and these effects are not strong enough to remove these particles from the resonance. Our numerical simulations showed that about 75 per cent of the initial set of arc particles, under the gravitational effects of Saturn, Mimas, and Aegaeon, collide with Aegaeon in 500 yr. Thus, Aegaeon acts as a sink for these arc particles.

The Cassini cameras observed a population of micrometre-sized particles located in the G ring arc. These tiny particles, 1–10 μm in radius (r), can be strongly influenced by the effects of the solar radiation force. Considering that the planet has its heliocentric position vector as \mathbf{r}_{sp} ($r_{sp} = |\mathbf{r}_{sp}|$) and velocity as \mathbf{V}_p , the solar radiation force (SRF) experienced by a circumplanetary particle is (Mignard 1984)

$$\mathbf{F} = \frac{\Phi A}{c} Q_{pr} \left\{ \left[1 - \frac{\mathbf{r}_{sp} \cdot \left(\frac{\mathbf{V}_p}{c} + \frac{\mathbf{V}}{c} \right)}{r_{sp}} \right] \frac{\mathbf{r}_{sp}}{r_{sp}} - \frac{\mathbf{V}_p + \mathbf{V}}{c} \right\}, \quad (1)$$

where c is the speed of light and \mathbf{V} is the velocity vector of the particle with respect to the planet. The particles’ cross-section is A , and we considered that they are made of ideal material which implies $Q_{pr} = 1$. In our model the planet is in a circular orbit, hence r_{sp} , the magnitude of \mathbf{V}_p and the solar flux Φ are constants. Furthermore, we assumed that the Sun lies in the equatorial plane of the planet (i.e. the obliquity of the planet was neglected), which is a simplification that does not change significantly the magnitude of the solar radiation force and saves computational time. We also disregarded secondary and, at least an order of magnitude, weaker effects such as the planetary light reflection and shadow, and the Yarkovsky effect (Hamilton 1996).

We do not include the effects of the plasma drag and the electromagnetic force. These forces are responsible to cause an outward drift of the particle and the precession of orbital pericentre, respectively (Sun et al. 2017; Burns, Hamilton & Showalter 2001). As discussed in more detail in Section 5, including these forces will probably further reduce the lifetimes of these particles.

The solar radiation force equation was decomposed and its components were included in the Mercury package (Sfair & Giulianti Winter 2009) in order to analyse the orbital evolution of particles with sizes of 1, 3, 5, and 10 μm in radius. These particles are also perturbed by the gravity of Mimas, Tethys, and Aegaeon, and the gravity coefficients of Saturn.

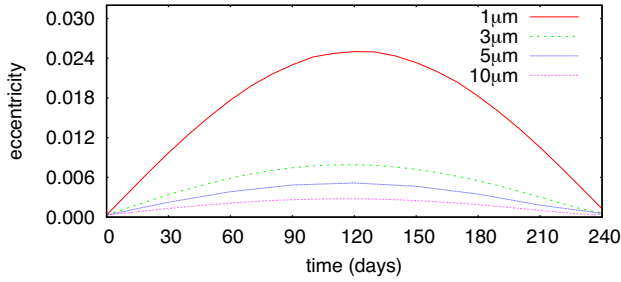


Figure 3. Time evolution of the geometric eccentricity of particles with different sizes due to the radiation pressure component. As the size of the particle increases, its Δe decreases.

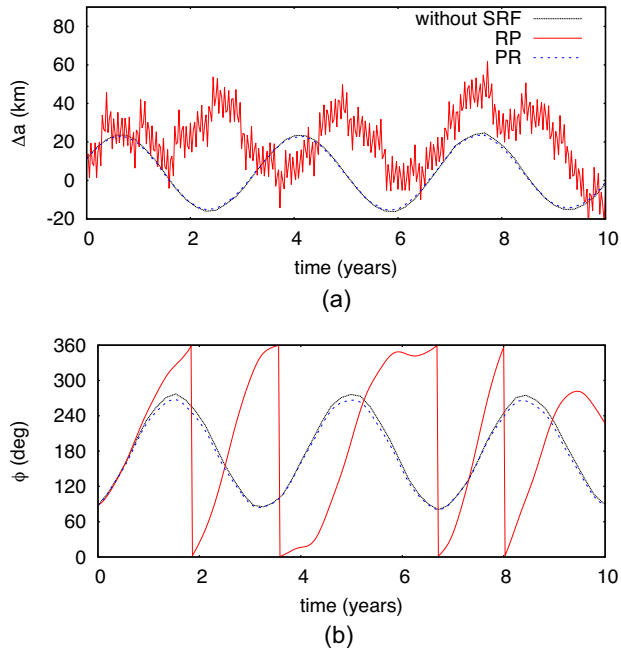


Figure 4. Time variation of (a) the difference between the semimajor axis of the particle and Aegaeon and (b) the resonant argument without the solar radiation force (SRF, dotted line), with the Poynting–Robertson component (dashed line) and with the radiation pressure (full line). The $1\ \mu\text{m}$ sized particle is initially with $\Delta a = 15\ \text{km}$ and has the same mean anomaly of Aegaeon.

The radiation pressure component (RP, the term that does not depend on the velocities in equation (1)) mainly causes a variation in the eccentricity of the particles which can be seen in Fig. 3. Each curve shows the time variation of the eccentricity of four particles, initially located at 10 km from the CER semimajor axis, with sizes of 1, 3, 5, and $10\ \mu\text{m}$ in radius. The smaller particle ($1\ \mu\text{m}$) has the larger variation in the eccentricity, from 0 to 10^{-2} . The $10\ \mu\text{m}$ sized particle has the smaller variation in the eccentricity, from 0 to 10^{-3} .

The radiation pressure component provokes, besides a variation in the eccentricity, short-period oscillations (about 40 d) in the semimajor axis of the particles, while the Poynting–Robertson component (PR, those terms velocity-dependent in equation 1) causes a slow decay of the semimajor axis, but in a time-scale much longer than the effects of the RP component. Fig. 4 shows the variation of the semimajor axis (Δa) and the resonant argument (ϕ) for a $1\ \mu\text{m}$ in radius particle initially with $\Delta a = 15\ \text{km}$, without the SRF and when considering each component separately. We can see that the effects of the Poynting–Robertson are negligible in this time-scale,

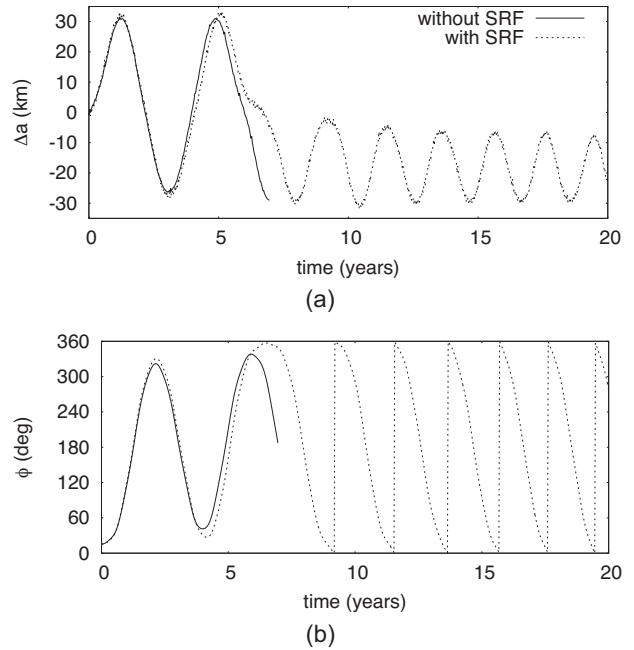


Figure 5. Time variation of (a) the difference between the semimajor axis of a $10\ \mu\text{m}$ sized particle and Aegaeon, and (b) the resonant argument with (dashed line) and without the SRF. In both cases the particle is located at the same semimajor axis of Aegaeon and displaced by $\Delta\lambda_0 = 20^\circ$.

while the radiation pressure component causes kilometre variations in the semimajor axis. For this particle, the variation in a is enough to remove the particle from the resonance in less than 2 yr.

Whether or not the particle remains in resonance may change its lifetime. Fig. 5 shows the difference between the semimajor axis of the particle and Aegaeon, and the resonant argument as a function of time for a $10\ \mu\text{m}$ sized particle, initially with the same semimajor axis ($\Delta a_0 = 0\ \text{km}$) of Aegaeon and mean anomaly displacement by $\Delta\lambda_0 = 20^\circ$, with (dashed line) and without the effects of the solar radiation force. When no solar radiation force is acting in the system, the particle is trapped in the 7:6 CER with Mimas until colliding with Aegaeon in less than 10 yr. The effects of the solar radiation force remove the particle from the resonance after about 10 yr, when the resonant argument starts to circulate, and the lifetime of the particle increases by a factor 2.

In some cases a particle remains trapped in the resonance, despite of the perturbation of the SRF. Fig. 6 shows the difference between the geometric semimajor axis of the particle and Aegaeon and the resonant argument of a representative particle with $10\ \mu\text{m}$ in radius, initially with $\Delta a_0 = -5\ \text{km}$ ($a = 167\,488\ \text{km}$) and $\Delta\lambda_0 = 0^\circ$ from Aegaeon. This particle remains trapped in the 7:6 CER with Mimas for almost 35 yr, until colliding with the satellite.

We also found some particles that leave the arc, as it is shown in Fig. 7 for a $10\ \mu\text{m}$ grain in radius, initially with $\Delta a_0 = 25\ \text{km}$ ($a = 167\,522\ \text{km}$) and $\Delta\lambda_0 = 0^\circ$. This particle leaves the 7:6 CER with Mimas after about 20 yr. After this, the semimajor axis starts to decrease due to the Poynting–Robertson component, and the particle moves away from the arc region to the inner edge of the G ring.

We then computed the percentage of particles which remain in resonance, and those that the resonance argument circulates. The first corresponds to the column ‘arc’ in Table 3, while the column ‘ring’ corresponds to the percentage of particles that leave the CER. It is also presented the time necessary to remove through collisions 90 per cent of the ‘arc’ particles (t_{90}).

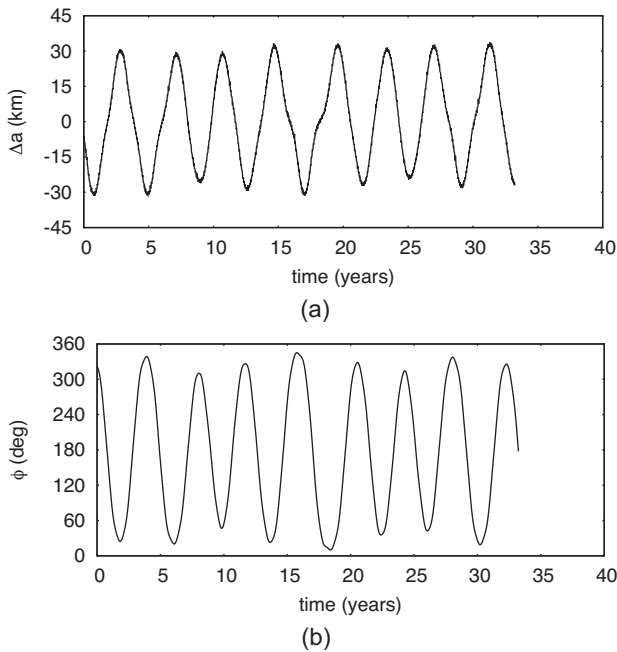


Figure 6. (a) The difference between the geometric semimajor axis of the particle and Aegaeon and (b) the resonant argument as a function of time in years for a $10\ \mu\text{m}$ sized particle initially at $\Delta a_0 = -5\ \text{km}$ and $\Delta \lambda_0 = 0^\circ$. The particle collides with the satellite in less than 35 yr.

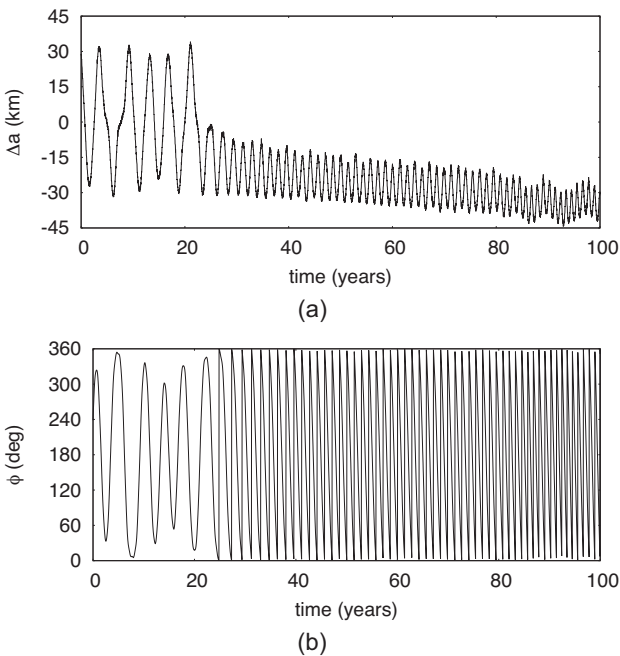


Figure 7. The same as Fig. 6 for a particle initially with $\Delta a_0 = 25\ \text{km}$ ($a = 167\,522\ \text{km}$) and $\Delta \lambda_0 = 0^\circ$.

Even though Aegaeon's and the particles' semimajor axes periodically cross due to the resonance, the excitation of the eccentricity caused by the SRF increases the number of times that the particles' orbital radius intersect the orbit of the satellite. Since the amplitude of the eccentricity varies inversely with the particles' size, it is expected that the smaller grains have a larger probability to leave the arc and also have a shorter lifetime. After 3 yr, more than 90 per cent of the $1\ \mu\text{m}$ particles collide with the satellite, while $10\ \mu\text{m}$ sized grains have longer lifetimes.

Table 3. Percentage of particles of different sizes that remain in the arc (in resonance) and those particles that leave the arc but remain in the G ring. The time (in years) necessary to 90 per cent of the total ensemble of particles, trapped in the arc, to be removed by collisions is shown in the last column.

$r\ (\mu\text{m})$	Arc (per cent)	Ring (per cent)	$t_{90}\ (\text{yr})$
1	55	45	3
3	58	42	9
5	60	40	16
10	64	36	26

Table 4. Summary of the numerical simulations considering particles of different sizes and ejection velocities. The particles were classified as *arc* when they remain the entire simulation in resonance and as *ring* otherwise. t_{90} corresponds to the time in years necessary to 90 per cent of the ensemble to be removed by collision.

		$1\ \mu\text{m}$	$3\ \mu\text{m}$	$5\ \mu\text{m}$	$10\ \mu\text{m}$
$1v_{\text{esc}}$	Arc	100 per cent	100 per cent	100 per cent	100 per cent
	t_{90}	2.5	4.6	14.4	38.2
	Ring	0 per cent	0 per cent	0 per cent	0 per cent
$5v_{\text{esc}}$	Arc	92 per cent	100 per cent	100 per cent	100 per cent
	t_{90}	3.0	12.6	20.6	36.7
	Ring	8 per cent	0 per cent	0 per cent	0 per cent
$10v_{\text{esc}}$	Arc	66.3 per cent	68.7 per cent	70.6 per cent	71.3 per cent
	t_{90}	3.4	13.9	22.5	41.9
	Ring	33.7 per cent	31.3 per cent	29.4 per cent	28.7 per cent
	t_{90}	35.0	94.9	136.3	278.6

3 PARTICLES EJECTED FROM AEGAEON'S SURFACE

Throughout the Solar system there is a flux of interplanetary dust particles (IDPs), which can be focused by the presence of a planet. While moving towards the planet, these IDPs can collide with a satellite at a speed of $\mathcal{O}(10\ \text{km s}^{-1})$, and if the satellite is small (radius up to a few tens of kilometres), the outcome of these hypervelocity impacts is the ejection of micrometric particles. Before calculating the amount of material produced by these collisions on Aegaeon surface (Section 4), we will analyse the orbital evolution of a set of particles ejected from its surface.

We considered particles with sizes of 1, 3, 5, and $10\ \mu\text{m}$ in radius, leaving the surface of the satellite with initial velocities equal to 1, 5, and 10 times the escape velocity of the satellite (v_{esc}). These parameters were chosen in a manner to cover the most likely distribution expected for the dust production mechanism (Krivov et al. 2003). Similarly to the previous section, the dust grains evolved under the influence of the planet and its gravity coefficients (J_2 , J_4 , and J_6), the gravitational effects of Mimas, Tethys, and Aegaeon, and also the solar radiation force. For each combination of particle size and ejection velocity, an ensemble of 1000 particles, launched at the same time, was analysed. All particles were launched radially away from Aegaeon and in the equatorial plane of Saturn. The angular position, related to the surface of the satellite, was randomly chosen from 0° to 360° with uniform probability.

Table 4 summarizes the outcome of the numerical simulations. We divided each sample into *arc* particles, corresponding to those remaining all the integration time in resonance (thus azimuthally confined), and the *ring* particles the ones that make excursions

through the ring. Since all particles hit the surface of Aegaeon we computed the time necessary to remove 90 per cent of each set (t_{90}).

The amount of particles that remain in the arc decreases slightly for smaller grains, but we note a substantial change when the ejection velocity increases. Smaller and faster grains are more likely to leave the arc and therefore they can survive longer. It is mainly caused by those particles that experience stronger variations in the semimajor axis due to the SRF and, as a consequence, they leave the resonance. At this point, those particles are classified as ‘ring’ and they present larger survival time since their orbital paths go further from the satellite.

When launched at lower speeds, the particles remain entirely confined in the arc. Their survival time is shorter since they stay closer to Aegaeon’s orbit. The longer lived ensemble is the one formed by the faster and larger grains, but even in this case the particles do not survive more than 300 yr.

4 MASS PRODUCTION RATE

Besides acting as a sink for the particles of the G ring/arc, Aegaeon can produce dust due to the impacts of interplanetary grains. Through the simplified model presented in Sfair & Giuliatti Winter (2012) we compute the mass production rate (M^+) due to the impacts of projectiles directly on to the surface of the satellite as

$$M^+ = F_{\text{imp}} Y S, \quad (2)$$

where F_{imp} is the mass flux of impactors that reaches the satellite, Y is the ejecta yield, and S is the satellite cross-section.

The characterization of the interplanetary dust grain environment is a difficult task, specially for the outer part of the Solar system due to the small number of direct measurements. Combining data from several missions, Poppe (2016) estimates that the mass flux at Saturn’s heliocentric distance is $1 \times 10^{-17} \text{ kg/(m}^2\text{s)}$. This value is enhanced by the gravitational focusing due to the planet, so that the effective flux at Aegaeon’s orbit is $F_{\text{imp}} \sim 5.5 \times 10^{-17} \text{ kg m}^2 \text{ s}^{-1}$. It was assumed that the radius of Aegaeon is 240 m, so its cross-section area is $\sim 1.8 \times 10^5 \text{ m}^2$.

The yield measures efficiency of the ejection process, and for a satellite with a pure ice surface (no silicates) it can be written as (Koschny & Grün 2011)

$$Y = 2.64 \times 10^{-5} m_{\text{imp}}^{0.23} v_{\text{imp}}^{2.46}. \quad (3)$$

For a typical impactor of 10^{-8} kg ($r \sim 100 \mu\text{m}$) with velocity of 23 km s^{-1} (after the gravitational focusing), the yield is $Y \sim 2 \times 10^4$.

By this mechanism, impacts with Aegaeon produce dust grains at a rate of

$$M^+ \sim 2 \times 10^{-7} \text{ kg s}^{-1}. \quad (4)$$

In order to determine if ejecta from Aegaeon can be the source of visible dust in the arc, it is necessary to estimate the mass of the arc. First, we assume a power law distribution for the particle size distribution as

$$dN = C r^{-q} dr, \quad (5)$$

where dN is the number of particles and $q = 3.5$ is assumed as a typical value. The optical depth can be written as

$$\tau = \int_{r_1}^{r_2} d\tau = \int_{r_1}^{r_2} \pi r^2 dN \quad (6)$$

and the mass of the dust can be calculated by Sfair & Giuliatti Winter (2012)

$$m = A_{\text{arc}} \left(\frac{4}{3} \pi \rho \right) \int_{r_1}^{r_2} r^3 dN, \quad (7)$$

where A_{arc} is the surface area of the arc. We assumed a simplified model considering the arc as a 60° circular sector with radius $167\,493 \pm 125 \text{ km}$. If we consider a uniform optical depth for the arc as $\tau = 10^{-5}$ (Hedman et al. 2007) and dominated by small ice particles ($r = [1 - 10] \mu\text{m}$), which is expected by the impact process, it gives $m \sim 2 \times 10^6 \text{ kg}$. This value is close to the high end of the dust mass estimates from Hedman et al. (2007).

Neglecting any loss mechanism, the total amount of dust in the arc would need about 30 000 years to accumulate. Since this time is at least three orders of magnitude larger than those presented in Table 4, it is unlikely that Aegaeon alone could keep the arc dust in a steady state.

5 DISCUSSION

The G ring arc region is a dynamic environment composed by dust particles, probably cm-m sized bodies, and a small satellite Aegaeon. The satellite and the particles are both trapped in a 7:6 CER with the satellite Mimas, responsible for keeping the particles and Aegaeon azimuthally confined in 60° of longitude. Besides the gravitational effects, the micrometre-sized dust particles are also strongly affected by the solar radiation force, which can lead them to collisions or ejection from the arc.

In this work, we analyse Aegaeon’s effects on the G-ring arc. In the numerical simulations the set of micrometre-sized particles is under the gravitational effects of the massive bodies Saturn, Mimas, Tethys, and Aegaeon. Our results showed that Aegaeon acts as a sink for the particles, removing them by collisions. About 75 per cent of the confined particles are removed from the arc in less than 500 yr.

The solar radiation component induces short period variations in the semimajor axis of the particles, which changes the resonant argument, and as a result most of the particles are removed from the resonance. This force also changes the eccentricities of the particles, leading to orbital crossing and eventually collisions between these particles and the satellite Aegaeon. The lifetime of 90 per cent of the initial set of $1 \mu\text{m}$ sized particles is about 3 yr, and 26 yr for particles $10 \mu\text{m}$ in radius. Therefore, the presence of Aegaeon reduces the lifetime of the particles leading to the extinction of the arc. This lifetime may be even shorter, since in our numerical simulations the plasma drag and the electromagnetic force were not taken into account. The former perturbation causes an outward drift (Sun et al. 2017), while the latter may increase even more the eccentricity of the particles (Hamilton 1993), thus both perturbations will probably cause particles to be removed from the arc even faster.

Hedman et al. (2009) argued that debris ejected from the surface of small satellites can stay confined in the same resonance of these satellites. Our results showed it is true for the particles ejected at slower velocities. However, the confined particles have a very short lifetime, 90 per cent of the entire population leave the arc in less than 20 yr. Only 8 per cent of the smaller particles goes to the G ring, the majority of them collide with the satellite Aegaeon. The longer lived ensemble is composed by larger particles leaving the surface of the satellite with $10v_{\text{esc}}$, these particles can last up to ~ 300 yr.

Although Aegaeon is below the optimum size to generate dust by impacts of interplanetary dust particles (Burns et al. 2001), we calculated the amount of dust this small satellite can contribute

to the arc population. Our result shows that Aegaeon can produce particles at a rate of $2 \times 10^{-7} \text{ kg s}^{-1}$, and if the mass of the arc is about $2 \times 10^6 \text{ kg}$, neglecting any loss mechanism, it would take more than 300 000 yr to Aegaeon populated the arc. Our simulations therefore show that Aegaeon is probably a net sink for arc particles.

Our simplified model takes into account only the direct process of dust. The assumed yield and interplanetary dust flux must be taken at least with one order of uncertainty. However, even considering a lower estimate for the arc mass and the upper limits for the flux and yield, the time necessary to accumulate such amount of dust is several orders of magnitude larger than the survival time of the particles.

In order to maintain the dust population in a steady state, additional processes must be invoked. For instance, there is evidence that the ring may be populated by multiple objects $\mathcal{O}(\text{cm-m})$ across, which are below the threshold level of the cameras to be detected. A more complex process involving secondary impacts of IDPs with these objects, or even impacts among themselves, could produce more dust particles than the primary impacts.

ACKNOWLEDGEMENTS

We would like to thank the anonymous reviewer who greatly improved the final text. The authors thank Fundação de Amparo à Pesquisa do Estado de São Paulo (Proc. 2016/24488-0 and Proc. 2106/24561-0) and Conselho Nacional de Desenvolvimento Científico e Tecnológico (Proc. 309714/2016-8 and Proc. 305737/2015-5) for the financial support.

REFERENCES

- Burns J. A., Hamilton D. P., Showalter M. S., 2001, Dusty rings and circumplanetary dust. In *Interplanetary Dust*. Springer Verlag, Berlin
- Chambers J. E., 1999, *MNRAS*, 304, 793
- El Moutamid M., Sicardy B., Renner S., 2014, *Celest. Mech. Dyn. Astron.*, 118, 235
- Hamilton D. P., 1993, *Icarus*, 101, 244
- Hamilton D. P., 1996, *Icarus*, 123, 503
- Hedman M. M., Burns J. A., Tiscareno M. S., Porco C. C., Jones G. H., Roussis E., Krupp N., Paranicas C., Kempf S., 2007, *Science*, 317, 653
- Hedman M. M., Murray C. D., Cooper N. J., Tiscareno M. S., Beurle K., Evans M. W., Burns J. A., 2009, *Icarus*, 199, 378
- Hedman M. M., Cooper N. J., Murray C. D., Beurle K., Evans M. W., Tiscareno M. S., Burns J. A., 2010, *Icarus*, 207, 433
- Koschny D., Grün E., 2011, *Icarus*, 154, 402
- Krivov A. V., Sremčević M., Spahn F., Dikarev V. V., Kholshchevnikov K. V., 2003, *Planet. Space Sci.*, 51, 251
- Mignard F., 1984. *Planetary rings*. Univ. Arizona Press, Tucson
- Poppe A. R., 2016, *Icarus*, 264, 369
- Renner S., Sicardy B., 2006, *Celest. Mech. Dyn. Astron.*, 94, 237
- Sfair R., Giuliatti Winter S. M., 2009, *A&A*, 505, 845
- Sfair R., Giuliatti Winter S. M., 2012, *A&A*, 543, 17
- Sun K. L., Seiß M., Hedman M. M., Spahn F., 2017, *Icarus*, 284, 206
- Thomas P. C., Burns J. A., Hedman M., Helfenstein P., Morrison S., Tiscareno M. S., Veverka J., 2013, *Icarus*, 226, 999

This paper has been typeset from a \LaTeX file prepared by the author.